

Parity breakdown, vortices, and dark soliton states in a Bose gas of resonantly excited polaritons

S. S. Gavrilov

*Institute of Solid State Physics RAS, 142432 Chernogolovka, Russia
National Research University Higher School of Economics, 101000 Moscow, Russia and
A. M. Prokhorov General Physics Institute RAS, 119991 Moscow, Russia*

(Dated: September 22, 2019)

A new mechanism of parity breakdown in a spinor Bose gas is predicted; it causes a single-mode state of polaritons to be spontaneously divided into different polarization domains which annihilate each other at the interface areas. In a polariton wire, such interface is a dark soliton that can run in space without dissipation. In a planar cavity, quantized vortices arise in which phase difference of orthogonally polarized components makes one complete turn around the core. Coupled vortex-antivortex pairs and straight filaments can form in analogy to Bose-Einstein condensates and superconductors. However, the rotational symmetry is broken even for individual vortices, which makes them interact on a large scale and form internally ordered structures. These states come into being under resonant excitation if the spin coupling rate significantly exceeds the decay rate.

Equilibrium Bose-Einstein condensates obey an autonomous $U(1)$ -invariant wave equation, but the very onset of macroscopic coherence is accompanied by symmetry breaking so that all particles share the same spontaneously chosen phase. When the symmetry has broken, the underlying phase freedom reveals itself in quantized vortices, topological excitations arising because of a weak Coulomb repulsion of particles. They were observed in various systems including quantum liquids [1, 2], superconductors [3], cold atoms [4, 5], and microcavities [6, 7]. Of particular interest are cavity polaritons, mixed states of photons and excitons formed in a thin quasi-two-dimensional layer of a semiconductor microcavity [8, 9]. Their coherent states originate in two ways, (i) via Bose-Einstein condensation from a nonresonantly pumped excitonic reservoir to the ground state or, thanks to the photonic component, (ii) directly under resonant and coherent optical driving [10]. In contrast to equilibrium systems, the directly driven condensate displays forced oscillations and its phase is not free but imposed by the pump wave. For this reason all known ways to excite vortices resonantly involve explicit patterning of the incident pump beam and/or intracavity resonance energy [11–20]. At the same time, nobody has seen vortices formed in a homogeneous Bose system continuously driven by a plane electromagnetic wave. This phenomenon is the subject of the current Letter.

We report a new kind of quantized vortices that originates specifically under the conditions of resonant excitation owing to spontaneous breakdown of the spin-reversal symmetry (parity). As will be shown below, parity breaks down when particles of opposite spin are linearly coupled. A homogeneous, spin-symmetric, and symmetrically driven initial state of a Bose gas is then divided into large-scale domains that differ in the way of symmetry breaking. Two equally possible steady states have opposite phases, so they annihilate each other and, consequently, the boundary between different domains is dilute and highly unstable. It gives birth to vortices in a two-dimensional system and dark solitons in a one-dimensional system. In some respects these excitations are very similar to their equilibrium counterparts, for instance, vortex-antivortex dipoles are easily formed on reaching a crossover point in

analogy to atomic gases ([21]). At the same time, vortices in the driven system can interact on a scale largely exceeding their healing length and thus form complex patterns with internal ordering. The polarization properties of such vortices are also uncommon and do not fit into the conventional row of the half- [22, 23], full-, and spin-vortex states [18] as well as linear-polarization vortices [19, 20].

Let us consider a planar polariton system excited at normal incidence (axis z) by a coherent light wave. Polaritons have two spin states matching two opposite directions of total angular momentum ($J_z = \pm 1$); they correspond to right- and left-handed circular polarizations of light. Opposite spin states do not interact pairwise if the driven mode is far below the exciton level [24, 25]. However, they can be linearly coupled owing to lifted degeneracy of eigenstates with orthogonal polarizations, which takes place in the presence of a mechanical stress [26–28] or constant magnetic field parallel to the cavity surface. Within the mean-field approach, this system is described by two amplitudes $\psi_{\pm}(\mathbf{r}, t)$ obeying the nonautonomous (“driven”) variant of the Gross-Pitaevskii equation [9],

$$i\hbar \frac{\partial \psi_{\pm}}{\partial t} = (\hat{E} - i\gamma + V\psi_{\pm}^* \psi_{\pm}) \psi_{\pm} + \frac{g}{2} \psi_{\mp} + f_{\pm} e^{-iE_p t/\hbar}. \quad (1)$$

Here, $\hat{E} = \hat{E}(-i\hbar\nabla)$ is the energy operator determined by the lower-polariton dispersion law $E(k)$ that is nearly parabolic for small in-plane wave numbers k ; γ is the decay rate, $V > 0$ is the polariton-polariton interaction constant, $g/2$ is the spin coupling rate. When $\psi_{\pm} \rightarrow 0$ and the cubic terms are negligible, the system is diagonalized by the unitary transformation $\psi_{\pm} = (\psi_x \mp i\psi_y)/\sqrt{2}$. The eigenstates at $f_{\pm} = 0$ are orthogonally polarized and their energy levels are $E_{x,y}(k) = E(k) \pm g/2$, so that $g = E_x - E_y$ for each k . The last term in Eq. (1) represents an effective pump force, where f_+ and f_- are proportional to the respective polarization components of the external electric field. The pump frequency E_p/\hbar is supposed to be moderately close to the resonance frequency of the driven polariton state with zero k .

Throughout this work we consider the case of spin-symmetric excitation ($f_+ = f_- = f$), so that the equations

for ψ_+ and ψ_- are exactly the same. Since the model is homogeneous, they always have one-mode solutions of the form $\psi_{\pm}(t) = \bar{\psi}_{\pm} e^{-iE_p t/\hbar}$, similar to forced oscillations of a dissipative pendulum. Amplitudes $\bar{\psi}_{\pm}$ obey time-independent equations

$$(D + i\gamma - V|\bar{\psi}_{\pm}|^2) \bar{\psi}_{\pm} - \frac{g}{2} \bar{\psi}_{\mp} = f, \quad (2)$$

where $D = E_p - E(k=0)$ is the pump detuning from the mean (unsplit) ground-state level. This system is multistable ([29]). Clearly it has spin-symmetric solutions with $\psi_+ = \psi_-$ for each f , which we henceforth denote as the Π states. They are linearly polarized in the x direction, i.e., in the same way as the incident pump. The orthogonal (y) component is not excited, so the full spinor problem is reduced to a scalar problem with different pump detuning $D' = D - g/2$. In particular, the Π states exhibit intrinsic bistability when $D' > \sqrt{3}\gamma$ [30, 31].

In order to demonstrate different types of solutions, let us equate the left sides of Eqs. (2), which gives

$$\frac{\bar{\psi}_-}{\bar{\psi}_+} = \frac{D + g/2 + i\gamma - V|\bar{\psi}_+|^2}{D + g/2 + i\gamma - V|\bar{\psi}_-|^2}. \quad (3)$$

It is seen that if $V|\bar{\psi}_{\pm}|^2 = D + g/2$, then $\bar{\psi}_{\mp} \propto \gamma$, so that the circular-polarization degree $S_1 = (|\bar{\psi}_+|^2 - |\bar{\psi}_-|^2)/(|\bar{\psi}_+|^2 + |\bar{\psi}_-|^2)$ nearly reaches ± 1 at small γ . This kind of steady states will be denoted as Σ_{\pm} . They were experimentally observed in a microcavity with $g \gtrsim \gamma$ [26–28].

The system also has another way of parity breaking which comes into play at greater g/γ and is directly responsible for vortices and dark solitons. Suppose $V|\bar{\psi}_{\pm}|^2 = D + g/2 \pm \delta$, so that Eq. (3) turns into

$$\frac{\bar{\psi}_-}{\bar{\psi}_+} = \frac{i\gamma - \delta}{i\gamma + \delta}. \quad (4)$$

Using these formulae, one can simplify Eq. (2) for $\bar{\psi}_+$. After taking the absolute value of both sides, it yields

$$\left(\gamma^2 + \delta^2 + \frac{\gamma^2 g^2}{\gamma^2 + \delta^2} \right) \left(D + \frac{g}{2} + \delta \right) = V f^2. \quad (5)$$

If $|\delta|$ is much smaller than g and D , one can drop δ in the second parentheses of Eq. (5) which is then reduced to a quadratic equation for $\gamma^2 + \delta^2$. The latter has positive roots starting with pump intensity

$$f_1^2 = \frac{2\gamma g}{V} \left(D + \frac{g}{2} \right), \quad (6)$$

where $\gamma^2 + \delta^2 = \gamma g$. The assumed smallness of $|\delta|$ is justified when $\gamma \ll g \sim D$, in which case the overall consideration based on Eq. (4) is self-consistent. Near the threshold point $f = f_1$ we have $\delta/g \rightarrow 0$ and $\delta/\gamma \rightarrow \infty$ if $\gamma/g \rightarrow 0$. In accordance with Eq. (4), $\bar{\psi}_-/\bar{\psi}_+ \rightarrow -1$, so that the field is polarized linearly in the y direction.

Being very small at the threshold, $|\delta|$ decreases still further with increasing f for one of two pairs of solutions of

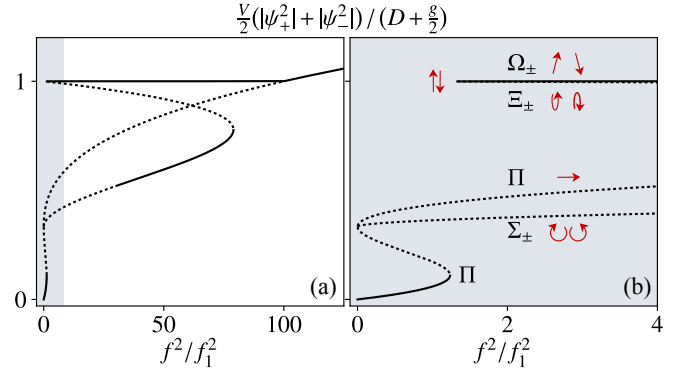


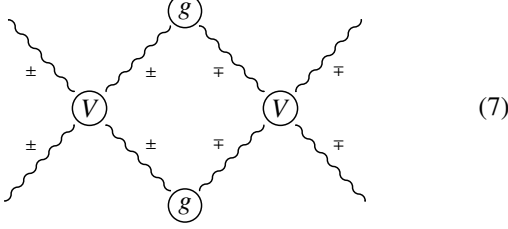
Figure 1. One-mode response functions [solutions of Eqs. (2)] at $\gamma = 5 \mu\text{eV}$ and $g = D = 1 \text{ meV}$, so that $f_2^2/f_1^2 = g/2\gamma = 100$. Dotted lines represent the solutions which are unstable even in the one-mode limit for $k = 0$. Panel (b) shows a magnified interval of (a) at small f ; arrows and ellipses schematically indicate polarization states.

Eq. (5). At $f \gg f_1$ we have $\delta(f) = \pm \gamma \sqrt{f_2^2/f^2 - 1}$, where $f_2^2 = (g/2\gamma)f_1^2$ is the upper threshold at which $|\delta|$ eventually turns to zero. Below this point, the condensate has constant total intensity $I = |\bar{\psi}_+|^2 + |\bar{\psi}_-|^2$ but varying polarization direction. The (x, y) polarization degree, $S_2 = (|\bar{\psi}_x|^2 - |\bar{\psi}_y|^2)/I$, shows a linear increase as a function of f^2 and ranges from about -1 at $f = f_1$ to $+1$ at $f = f_2$. The solutions with mutually opposite δ are distinguished by the sign of the “diagonal” linear polarization $S_3 = (\bar{\psi}_x^* \bar{\psi}_y + \bar{\psi}_y^* \bar{\psi}_x)/I$. Since the length of the Stokes vector (S_1, S_2, S_3) is unity and its circular-polarization component $S_1 = \delta/(D + g/2)$ is negligible, we have $S_3 \approx \pm \sqrt{1 - S_2^2}$ and, in particular, $S_3 \approx \pm 1$ at $f^2 = (f_1^2 + f_2^2)/2$. Let us denote this doublet of solutions as Ω_{\pm} . At the upper threshold, the Ω_{\pm} branches degenerate into the singlet Π branch, as it is seen from Fig. 1 in which all solutions of Eq. (2) are represented.

In a cousin doublet of solutions, henceforth Ξ_{\pm} , the value of $|\delta|$ grows with f , so the field gradually acquires noticeable right- or left-handed circular polarization. Since then ratio (4) does not satisfy Eqs. (2) even approximately. As seen in Fig. 1, the intensity of the Ξ states decreases with increasing f , which is indicative of instability. Sooner or later the Ξ doublet meets the Σ doublet and they both terminate.

The key point is that the Ω doublet is the only possible type of steady states in a wide interval of f^2 when $\gamma \ll g \sim D$. The instabilities of the Π and Σ_{\pm} states were investigated earlier, and here we only briefly remind the main results. The spin-symmetric Π state is unstable because an indefinitely small imbalance of $|\psi_+|$ and $|\psi_-|$ makes the greater component grow further by simultaneously suppressing the minor one [26–28, 32, 33]. This occurs at $g \gtrsim \gamma$ and leads to one of the Σ_{\pm} states. After one of the spin components has been suppressed by the other, a significant increase in the pump intensity is required for driving it up again, so that the length of the Σ branches in a diagram like Fig. 1 is quite great. Notice as well that the Josephson oscillations ([34]) are not possible in our system so long as both spin components have the same

“forced” frequency E_p/\hbar and, consequently, their phase difference does not vary with time. On the other hand, the pair interaction conserves spin and, taken alone, it also cannot help restore spin symmetry. However, the Σ branches lose stability with respect to a higher-order loop interaction process



—which simultaneously enables spins to be reversed and lifts the frequency degeneracy. Even when the condensate at $E = E_p$ has a perfectly circular polarization, new energy levels with different polarizations get populated at $E \approx E_p \pm D$ in a finite interval of k around $k = 0$. This process starts at $g \approx 4\gamma$ [35] and leaves no one-mode solutions within a certain range of f^2 , which results in turbulence [36], periodic spin networks, and chimera states [37].

Given that $g \sim D > 0$, a decrease in the decay rate γ broadens the interval of f^2 in which all of the Π and Σ_{\pm} states are forbidden. Simultaneously it lowers the critical point $f_1^2 \propto \gamma$ where the Ω_{\pm} states appear. They have the greatest intensity for each $f < f_2$ and are always stable.

The $\Pi \rightarrow \Omega$ transition is qualitatively different from the $\Pi \rightarrow \Sigma$ transition observed at $g \sim \gamma$. First, the superposition of Ω_+ and Ω_- has extremely low intensity near $f = f_1$. To make it clear, notice that replacing ψ_+ with ψ_- and vice versa turns Ω_+ into Ω_- and Σ_+ into Σ_- in view of symmetry. Thus, the average state for each doublet is spin-symmetric and must have the x polarization direction ($S_2 = +1$). We have found, however, that the Ω_{\pm} states are nearly y -polarized at $f = f_1$, so they simply annihilate each other, which also applies to the Ξ_{\pm} pair. That is why a turnover point between Ω_+ and Ω_- can behave like a dark soliton or vortex core.

Second, notice that the outcome of the $\Pi \rightarrow \Sigma_{\pm}$ transition at $g \sim \gamma$ is determined in its very beginning by the sign of $|\psi_+| - |\psi_-|$. By contrast, nothing determines the outcome of the $\Pi \rightarrow \Omega_{\pm}$ transition near $f = f_1$ at its early stage, because processes of the type (7) make a continuum of different k -states populated concurrently. After the spin symmetry has broken, the system goes through the stage of very strong spatiotemporal disorder. That is why vortices and dark solitons arise truly spontaneously, i. e., owing to infinitesimal fluctuations rather than finite seeding inhomogeneities.

The following numerical experiments are performed with typical parameters of a GaAs-based microcavity. The exciton-photon detuning at $k = 0$ is zero, the full Rabi splitting is 10 meV, the exciton mass is much greater than the photon mass $\epsilon E/c^2$, where $\epsilon = 12.5$ and $E = 1.5$ eV. Interaction constant V can be chosen arbitrarily, as it only determines threshold (6) for given γ , g , and D . A white-noise term is added to the right side of Eqs. (1) to simulate quantum fluctuations;

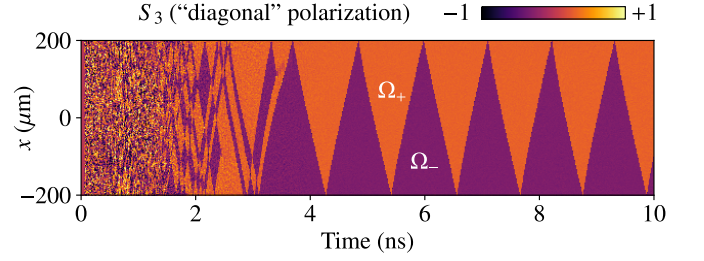


Figure 2. Solution of Eqs. (1) at $\gamma = 1 \mu\text{eV}$, $g = D = 1 \text{ meV}$, and $f^2/f_1^2 = 11$ in the one-dimensional case. The boundary between the Ω_{\pm} states behaves as a dark soliton; it runs with a constant speed and gets reflected from the 2-meV high potential walls at $x = \pm 200 \mu\text{m}$.

taken alone, it brings about a 10^9 times smaller average population $|\psi_{\pm}|^2$ than that induced by the regular pumping. The pump is smoothly switched on during 0.1 ns and then held constant. The boundary conditions are arranged by means of a sharp increase in the polariton energy (which renders the pump off-resonant) or decay rate.

Figure 2 shows a $400 \mu\text{m}$ long one-dimensional polariton system with potential walls near the boundaries. After the stage of disorder, this system nearly approaches equilibrium but remains two-component; it tends to be in the Ω state but does not prefer one of the Ω twins over the other. Each pair of the Ω_{\pm} domains are separated by a dark soliton, point-like interface at which total intensity I significantly drops down. When γ/g is especially small and f close to f_1 , such soliton

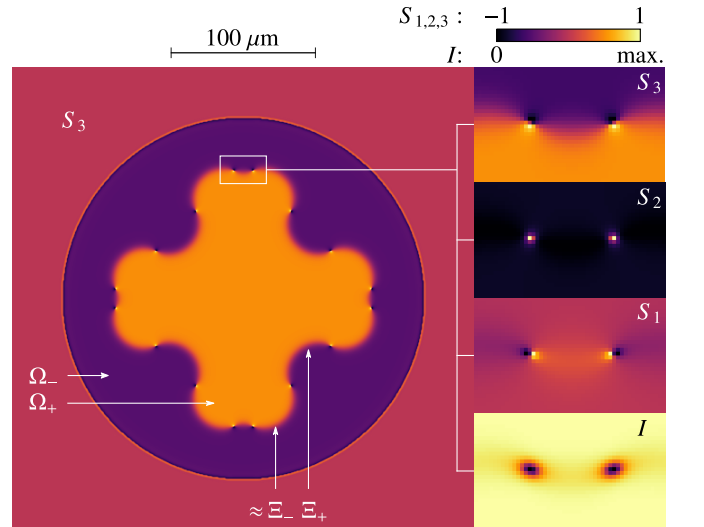


Figure 3. Intensity I and polarization degrees (normalized Stokes parameters) $S_{1,2,3}$ for a steady solution of Eqs. (1) formed in about 1 ns at $f^2/f_1^2 \approx 6.8$. Parameters γ , g , and D correspond to Fig. 1. In order to avoid a chaotic stage of evolution and retain symmetry, the initial conditions were biased to the Ω_+ and Ω_- states at $|\mathbf{r}| \leq 20 \mu\text{m}$ and $|\mathbf{r}| > 20 \mu\text{m}$, respectively, $\mathbf{r} = 0$ being the grid center. To ensure zero boundary conditions, γ is increased up to 4 meV at $|\mathbf{r}| = 125 \mu\text{m}$. Insets show a magnified fragment which contains two vortices with opposite topological charges.

can endlessly run and even reflect from the potential walls. Colliding solitons cancel each other, thus, only one can survive in the long term, resulting in a very unusual type of spatiotemporal self-pulsations seen in Fig. 2. Increasing f makes solitons fixed in space, so that the field becomes randomly divided into static polarization domains with alternating Ω_{\pm} . In the latter case, which is also typical of comparatively large values of γ/g , opposite Ω_+ and Ω_- states can be manually toggled back and forth by additional short-term excitation pulses.

The two-dimensional case (Fig. 3) is essentially more complex. Of particular interest is the boundary between the Ω_{\pm} states, its shape and polarization. To skip the turbulent stage, we have used rotationally symmetric initial conditions biased to the Ω_+ and Ω_- states, respectively, inside and outside a circle located at the grid center. Accordingly, the pump was not “switched on” smoothly but had just a fixed amplitude. Figure 3 shows the steady state to which such a system came after about 1 ns of evolution.

Here, the borderline between Ω_+ and Ω_- comprises 16 curved segments whose polarizations appear to be very close to the Ξ states. They alternate each other and tend to move in opposite directions from Ω_+ to Ω_- for Ξ_{\pm} . Each turnover point between Ξ_+ and Ξ_- naturally carries a vortex core and has very low intensity. Neighboring vortices with opposite rotation directions balance each other and help stabilize the system. The steady states like that represented in Fig. 3 are always internally balanced. However, in many cases the system does not come to a steady state even in tens of nanoseconds.

The Stokes vector components shown in Fig. 3 allow one to deduce the phase distribution around the core. It is seen that $S_1 \sim \pm 1$ and $S_3 \sim \pm 1$, respectively, along the tangent and the normal to the borderline at the core point. The signs of S_3 and S_1 match the Ω_{\pm} domains and Ξ_{\pm} segments. A purely circular polarization $S_1 = \pm 1$ implies that (i) $|\psi_+| = |\psi_-|$ and (ii) the (x, y) phase difference $\Delta\phi = \arg(\psi_x^* \psi_y)$ is equal to $\pi/2$ or $3\pi/2$, whereas $S_3 = \pm 1$ implies $\Delta\phi = 0$ or π . Thus, $\Delta\phi$ makes an angle of $\pm 2\pi$ around the core. At the same time, the orientation of the $S_{1,3}$ poles of each vortex is certain and corresponds to the long-range symmetry breaking. Static vortices of this kind can hardly bear topological charges other than ± 1 .

When two vortices of opposite charge come within short distances of each other, the borderline segment they bound becomes straight. In fact many adjacent vortices may cancel their high- S_1 poles and unite into straight Ω -neutral filaments which do not move in space. At larger f/f_1 , when the average of Ω_+ and Ω_- acquires a noticeably nonzero I , this new kind of the borderline is highly preferred over the Ξ states. The whole picture turns out to be steadily divided into several Ω_{\pm} domains by straight yet randomly directed lines which are analogous to fixed dark solitons formed in the one-dimensional system. The same occurs at comparatively large γ/g when Ω_+ and Ω_- do not annihilate each other completely even at $f = f_1$.

Figure 4 and video files [38] and [39] illustrate a crossover from the filaments to individual vortices analogous to the transition discovered by Berezinskii, Kosterlitz, and Thouless

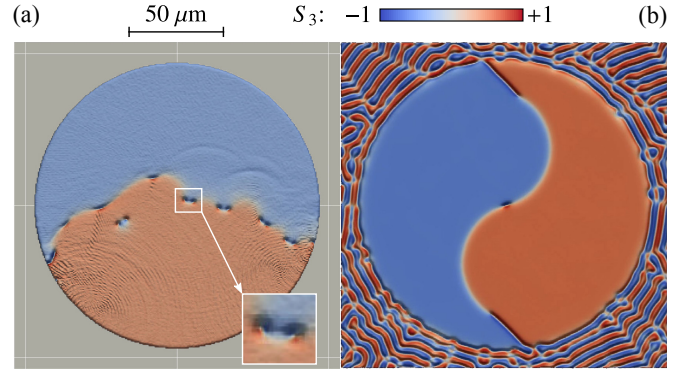


Figure 4. Snapshots of unsteady solutions of Eqs. (1). Parameters γ , g , and D correspond to Fig. 1. The value of f^2/f_1^2 is 6.8 for (a) and 13 for (b). The initial conditions are homogeneous (zero) in both cases. In (a), the boundary conditions are zero thanks to a high potential wall at $|r| = 75 \mu\text{m}$. No walls are present in (b), but γ is increased up to 0.2 meV at the same $|r|$, which results in a filamented field distribution [36] in the outer area; the boundary conditions are periodic. The obtained pattern steadily rotates clock-wise and makes a complete turn in 2.6 ns. Supplemental Materials [38, 39] contain video files showing the evolution of (a) and (b).

(BKT) [40, 41]. Both patterns (a) and (b) form spontaneously; the initial conditions are zero. In Fig. 4(a), the field is enclosed by a ring-shaped potential wall, so that polaritons can reflect from the boundary similar to Fig. 2. The Ξ -state borderline has $S_2 \sim -1$ and runs in space freely. However, at some places it occasionally turns into the said filaments with smaller I and larger S_2 sandwiched between the states with $S_3 \sim \pm 1$. The filaments slow down and break into the vortex-antivortex molecules which have small lifetime but freely penetrate into the Ω domains, in contrast to single vortices which are merely pinned to the borderline.

Instead of erecting a wall, in Fig. 4(b) we have increased the decay rate γ from $5 \mu\text{eV}$ to $200 \mu\text{eV}$ at the same boundary. In the outer area, the pump no longer reaches threshold (6), however, the Σ_{\pm} and Π states are still unstable. Consequently, the condensate wave vector is uncertain and the field has to be inhomogeneous on the scale $a \sim k_0^{-1}$, where $\hbar^2 k_0^2/2m = D + g/2$ and m is the polariton mass near $k = 0$. In the one-dimensional case, this would have resulted in a stiffly ordered dipolar network [37], but the two-dimensional system has more freedom and arranges itself into a labyrinthine structure like those discussed in Ref. [36]. It has $S_3 \sim \pm 1$ at the intensity maxima and $S_2 = +1$ at the minima and thus can be thought of as a host of vortex filaments in which vortices are tightly coupled (frozen) and do not manifest themselves in a usual manner. The inner disk-shaped area contains a single vortex at the center, two curved Ξ segments with $S_2 \sim -1$, and two straight filaments with $S_2 \sim +1$ connected to the outer labyrinth. This pattern rotates at a constant angular velocity and represents an instance of unsteady but fully established and self-consistent polariton states. It is “driven” by the instability of the Ξ segments which drift in the same angular direction. Such picture resembles Yin and Yang, the symbol of duality.

In summary, we have found a new class of many-body polariton states which are spontaneously formed owing to parity breakdown under resonant excitation. They are analogous to quantized vortices in Bose-Einstein condensates and superconductors in that they feature phase singularity and a BKT-like crossover. However, their collective properties are different because of a large-scale instability of the borderline between opposite Ω domains. The rotational symmetry of each vortex is broken and the ordering scale on which it has a pronounced effect on its environment appears to be much greater than the healing length. In certain cases a dilute Bose gas even displays an effectively rigid-body type of rotation. To create such states, one needs a microcavity in which decay rate γ is much smaller than the spin coupling rate. The excitation threshold f_1 (6) is expected to decrease with γ , which gives reason to hope that the discussed phenomena are feasible even in very high- Q microcavities. Notice, however, that the system considered is not reduced to an equilibrium Bose-Einstein condensate in the limit of $\gamma \rightarrow 0$ and $f_1 \rightarrow 0$ because the Ω states always oscillate at the pump frequency.

I am grateful to V.D. Kulakovskii, S.G. Tikhodeev, and N.A. Gippius for stimulating discussions. The work was supported by the Russian Science Foundation grant 16-12-10538.

-
- [1] L. Pitaevskii and S. Stringari, *Bose-Einstein Condensation and Superfluidity* (Oxford University Press, New York, 2016).
 - [2] A. J. Leggett, *Quantum Liquids: Bose Condensation and Cooper Pairing in Condensed-Matter Systems* (Oxford University Press, New York, 2006).
 - [3] G. Blatter, M. V. Feigel'man, V. B. Geshkenbein, A. I. Larkin, and V. M. Vinokur, *Rev. Mod. Phys.* **66**, 1125 (1994).
 - [4] M. R. Matthews, B. P. Anderson, P. C. Haljan, D. S. Hall, C. E. Wieman, and E. A. Cornell, *Phys. Rev. Lett.* **83**, 2498 (1999).
 - [5] C. N. Weiler, T. W. Neely, D. R. Scherer, A. S. Bradley, M. J. Davis, and B. P. Anderson, *Nature* **455**, 948 (2008).
 - [6] J. Scheuer and M. Orenstein, *Science* **285**, 230 (1999).
 - [7] K. G. Lagoudakis, M. Wouters, M. Richard, A. Baas, I. Carusotto, R. André, L. S. Dang, and B. Deveaud, *Nat. Phys.* **4**, 706 (2008).
 - [8] Y. Yamamoto, T. Tassone, and H. Cao, *Semiconductor Cavity Quantum Electrodynamics* (Springer-Verlag, Berlin, 2000).
 - [9] A. V. Kavokin, J. J. Baumberg, G. Malpuech, and P. Laussy, *Microcavities*, 2nd ed. (Oxford University Press, New York, 2017).
 - [10] A. Baas, J.-P. Karr, M. Romanelli, A. Bramati, and E. Giacobino, *Phys. Rev. Lett.* **96**, 176401 (2006).
 - [11] D. Whittaker, *Superlattices Microstruct.* **41**, 297 (2007).
 - [12] F. M. Marchetti, M. H. Szymańska, C. Tejedor, and D. M. Whittaker, *Phys. Rev. Lett.* **105**, 063902 (2010).
 - [13] D. N. Krizhanovskii, D. M. Whittaker, R. A. Bradley, K. Guda, D. Sarkar, D. Sanvitto, L. Viña, E. Cerda, P. Santos, K. Biermann, R. Hey, and M. S. Skolnick, *Phys. Rev. Lett.* **104**, 126402 (2010).
 - [14] D. Sanvitto, F. M. Marchetti, M. H. Szymanska, G. Tosi, M. Baudisch, F. P. Laussy, D. N. Krizhanovskii, M. S. Skolnick, L. Marrucci, A. Lemaître, J. Bloch, C. Tejedor, and L. Viña, *Nat. Phys.* **6**, 527 (2010).
 - [15] D. Sanvitto, S. Pigeon, A. Amo, D. Ballarini, M. De Giorgi, I. Carusotto, R. Hivet, F. Pisanello, V. G. Sala, P. S. S. Guimaraes, R. Houdré, E. Giacobino, C. Ciuti, A. Bramati, and G. Gigli, *Nat. Photon.* **5**, 610 (2011).
 - [16] L. Dominici, G. Dagvadorj, J. M. Fellows, D. Ballarini, M. De Giorgi, F. M. Marchetti, B. Piccirillo, L. Marrucci, A. Bramati, G. Gigli, M. H. Szymańska, and D. Sanvitto, *Science Advances* **1**, 10.1126/sciadv.1500807 (2015).
 - [17] T. Boulier, H. Terças, D. D. Solnyshkov, Q. Glorieux, E. Giacobino, G. Malpuech, and A. Bramati, *Sci. Rep.* **5**, 9230 (2015).
 - [18] L. Dominici, R. Carretero-González, A. Gianfrate, J. Cuevas-Maraver, A. S. Rodrigues, D. J. Frantzeskakis, G. Lerario, D. Ballarini, M. De Giorgi, G. Gigli, P. G. Kevrekidis, and D. Sanvitto, *Nat. Commun.* **9**, 1467 (2018).
 - [19] T. C. H. Liew, A. V. Kavokin, and I. A. Shelykh, *Phys. Rev. B* **75**, 241301 (2007).
 - [20] T. C. H. Liew, Y. G. Rubo, and A. V. Kavokin, *Phys. Rev. Lett.* **101**, 187401 (2008).
 - [21] T. W. Neely, E. C. Samson, A. S. Bradley, M. J. Davis, and B. P. Anderson, *Phys. Rev. Lett.* **104**, 160401 (2010).
 - [22] Y. G. Rubo, *Phys. Rev. Lett.* **99**, 106401 (2007).
 - [23] K. G. Lagoudakis, T. Ostatnický, A. V. Kavokin, Y. G. Rubo, R. André, and B. Deveaud-Plédran, *Science* **326**, 974 (2009).
 - [24] A. V. Sekretenko, S. S. Gavrilov, and V. D. Kulakovskii, *Phys. Rev. B* **88**, 195302 (2013).
 - [25] M. Vladimirova, S. Cronenberger, D. Scalbert, K. V. Kavokin, A. Miard, A. Lemaître, J. Bloch, D. Solnyshkov, G. Malpuech, and A. V. Kavokin, *Phys. Rev. B* **82**, 075301 (2010).
 - [26] S. S. Gavrilov, A. V. Sekretenko, S. I. Novikov, C. Schneider, S. Höfling, M. Kamp, A. Forchel, and V. D. Kulakovskii, *Appl. Phys. Lett.* **102**, 011104 (2013).
 - [27] A. V. Sekretenko, S. S. Gavrilov, S. I. Novikov, V. D. Kulakovskii, S. Höfling, C. Schneider, M. Kamp, and A. Forchel, *Phys. Rev. B* **88**, 205302 (2013).
 - [28] S. S. Gavrilov, A. S. Bichkin, S. I. Novikov, S. Höfling, C. Schneider, M. Kamp, A. Forchel, and V. D. Kulakovskii, *Phys. Rev. B* **90**, 235309 (2014).
 - [29] N. A. Gippius, I. A. Shelykh, D. D. Solnyshkov, S. S. Gavrilov, Y. G. Rubo, A. V. Kavokin, S. G. Tikhodeev, and G. Malpuech, *Phys. Rev. Lett.* **98**, 236401 (2007).
 - [30] V. F. Elesin and Y. V. Kopaev, *Sov. Phys. JETP* **36**, 767 (1973).
 - [31] A. Baas, J. P. Karr, H. Eleuch, and E. Giacobino, *Phys. Rev. A* **69**, 023809 (2004).
 - [32] S. S. Gavrilov, A. A. Demenev, and V. D. Kulakovskii, *JETP Lett.* **100**, 817 (2015).
 - [33] S. S. Gavrilov and V. D. Kulakovskii, *JETP Lett.* **104**, 827 (2016).
 - [34] I. A. Shelykh, D. D. Solnyshkov, G. Pavlovic, and G. Malpuech, *Phys. Rev. B* **78**, 041302 (2008).
 - [35] S. S. Gavrilov, *JETP Lett.* **105**, 200 (2017).
 - [36] S. S. Gavrilov, *Phys. Rev. B* **94**, 195310 (2016).
 - [37] S. S. Gavrilov, *Phys. Rev. Lett.* **120**, 033901 (2018).
 - [38] Supplemental material showing the evolution of Fig. 4(a), https://drive.google.com/open?id=1R3L5zq_g1J4V0DxrT7sFwXiPnxM0cCG.
 - [39] Supplemental material showing the evolution of Fig. 4(b), https://drive.google.com/open?id=1L1tcihsBJ_FyCxJG_bveh5ByILizI7r0.
 - [40] J. M. Kosterlitz and D. J. Thouless, *J. Phys. C* **6**, 1181 (1973).
 - [41] Z. Hadzibabic, P. Krüger, M. Cheneau, B. Battelier, and J. Dalibard, *Nature* **441**, 1118 (2006).